Cement & Concrete Composites 45 (2014) 125–135

Contents lists available at ScienceDirect

Cement & Concrete Composites

journal homepage: www.elsevier.com/locate/cemconcomp

Modification of phase evolution in alkali-activated blast furnace slag by the incorporation of fly ash

Idawati Ismail [a,b], Susan A. Bernal [a,c], John L. Provis [a,c,*], Rackel San Nicolas [a], Sinin Hamdan [b], Jannie S.J. van Deventer [a,d]

[a] Department of Chemical and Biomolecular Engineering, University of Melbourne, Victoria 3010, Australia
[b] Faculty of Engineering, Universiti Malaysia Sarawak, Kota Samarahan 94300, Sarawak, Malaysia
[c] Department of Materials Science and Engineering, University of Sheffield, Sir Robert Hadfield Building, Mappin St., Sheffield S1 3JD, United Kingdom
[d] Zeobond Pty. Ltd., P.O. Box 23450, Docklands, Victoria 8012, Australia

ARTICLE INFO

Article history:
Received 25 January 2013
Received in revised form 10 July 2013
Accepted 13 September 2013
Available online 20 September 2013

Keywords:
Alkali-activated slag
Fly ash geopolymer
Curing time
Gel composition
Microstructure

ABSTRACT

The microstructural evolution of alkali-activated binders based on blast furnace slag, fly ash and their blends during the first six months of sealed curing is assessed. The nature of the main binding gels in these blends shows distinct characteristics with respect to binder composition. It is evident that the incorporation of fly ash as an additional source of alumina and silica, but not calcium, in activated slag binders affects the mechanism and rate of formation of the main binding gels. The rate of formation of the main binding gel phases depends strongly on fly ash content. Pastes based solely on silicate-activated slag show a structure dominated by a C–A–S–H type gel, while silicate-activated fly ash are dominated by N–A–S–H 'geopolymer' gel. Blended slag-fly ash binders can demonstrate the formation of co-existing C–A–S–H and geopolymer gels, which are clearly distinguishable at earlier age when the binder contains no more than 75 wt.% fly ash. The separation in chemistry between different regions of the gel becomes less distinct at longer age. With a slower overall reaction rate, a 1:1 slag:fly ash system shares more microstructural features with a slag-based binder than a fly ash-based binder, indicating the strong influence of calcium on the gel chemistry, particularly with regard to the bound water environments within the gel. However, in systems with similar or lower slag content, a hybrid type gel described as N–(C)–A–S–H is also identified, as part of the Ca released by slag dissolution is incorporated into the N–A–S–H type gel resulting from fly ash activation. Fly ash-based binders exhibit a slower reaction compared to activated-slag pastes, but extended times of curing promote the formation of more cross-linked binding products and a denser microstructure. This mechanism is slower for samples with lower slag content, emphasizing the correct selection of binder proportions in promoting a well-densified, durable solid microstructure.

1. Introduction

Climate change is a global issue, and many countries are committing to reduce their emissions of greenhouse gases to reduce their environmental impact. The fact that the production of one tonne of Portland cement generates almost one tonne of carbon dioxide leads to the urgent need to search for alternative materials for the partial or total replacement of Portland cement with reduced carbon footprint [1]. This has been one of the main drivers for the development of alternative clinker-free binders, such as alkali-activated binders including 'geopolymers', which are produced at room temperature through the reaction between an aluminosilicate precursor and an alkaline activator, to promote the dissolution and consequent polycondensation of binding phases to form a hardened material with good mechanical strength and durability [2,3].

Fly ash and blast furnace slag are the most popular choices as main raw materials in the production of alkali-activated materials, and their activation has been extensively studied over the past decades [4–9]. Marked structural, mechanical and physical differences have been identified in activated binders using precursors from different sources, as a consequence of the chemical and physical differences between slag and fly ash precursors and the influences of different activator concentrations and chemistries, and the microstructures of alkali-activated slag and of fly ash geopolymers have been extensively studied in systems based on sole precursors. The alkali activation of slag involves the dissolution

* Corresponding author at: Department of Materials Science and Engineering, University of Sheffield, Sir Robert Hadfield Building, Mappin St., Sheffield S1 3JD, United Kingdom. Tel.: +44 114 222 5490; fax: +44 114 222 5943.
E-mail address: j.provis@sheffield.ac.uk (J.L. Provis).

0958-9465/$ - see front matter © 2013 Elsevier Ltd. All rights reserved.
http://dx.doi.org/10.1016/j.cemconcomp.2013.09.006

of calcium and participation of Al to form a C–(A)–S–H type gel [10–12], promoting the development of high mechanical strength and durability in these systems [13–16]. On the other hand, strength development in alkali-activated aluminosilicate binders is provided by the formation of a three dimensional "N–A–S–H" type gel i.e. a sodium aluminosilicate gel forms as the main reaction product in these systems [17,18].

The use of slag and fly ash together to form an alkali-activated binder will generally lead to formation of a high amount of tetracoordinated Al charge-balanced by Na, and binder gels in the hydrated Na_2O–CaO–Al_2O_3–SiO_2 system. The nature of the main type of gel formed when both precursors are activated depends on various factors such as activator type and concentration, and the relative amounts of fly ash and slag. In general, dissolution of slag and fly ash upon alkali activation can produce a higher degree of cross-linking in binder systems consisting of both C–A–S–H and N–A–S–H gels. Lloyd [19], assessing the structure of different activated slag/fly ash blends, identified that increasing the amount of slag as a calcium source will lead to the formation of C–S–H products with certain degrees of aluminum substitution, depending on the availability of this element in the fly ash and slag. Escalante García et al. [20] identified an optimal activator modulus (SiO_2/Na_2O ratio) of around 1.0–1.5 for a 1:1 blend of fly ash and slag, as a consequence of the scope for coexistence of both C–S–H and N–A–S–H in the system. Kumar et al. investigated the effect of slag replacement in fly ash geopolymers in the kinetics of reaction, finding that the C–S–H gel dominates the reaction products, coexisting with aluminosilicate gels, resulting in improved setting properties and higher compressive strength with slag addition [21,22]. The X-ray microtomography data of Provis et al. [23] show a similar dominance of slag on a microstructural level, as the 1:1 blend of fly ash and slag in that investigation displayed trends in porosity which were more similar to a slag-based binder than a fly ash-based binder. Microstructural observation of younger-age pastes by Yang et al. [24] also showed that partial slag substitution in sodium hydroxide-based fly ash geopolymers improves strength and affects the reaction mechanism controlling the formation of the main binding gels.

Despite these previous studies, an in-depth understanding of the mechanism of incorporation of fly ash in activated slag binders, and the associated effects on longer term evolution of microstructure, is still lacking. The knowledge of microstructural development of activated binders using fly ash and slag as precursors is limited to relatively immature samples, while it is known that changes in the binder phase can proceed even at an advanced curing age [25]. The dissolution of fly ash in an activated slag binder may take longer, and this justifies investigation well beyond the most commonly studied curing age of 28 days. It is vital to understand the evolution of phases over time for various mix proportions of fly ash and slag in order to design for specific strengths or to ensure durability. Therefore, this study will characterize the microstructural changes taking place in alkali-activated slag/fly ash binders up to the age of 180 days, using X-ray diffraction, infrared spectroscopy, thermogravimetry and scanning electron microscopy.

2. Experimental methods

2.1. Materials

The geopolymer precursors used in this investigation were a fly ash (FA), Class F according to ASTM C 618, from Bayswater Power Station, New South Wales, Australia, and a granulated blast furnace slag (GBFS) supplied by Zeobond Pty Ltd, Australia. The oxide compositions of the precursors are given in Table 1. It is notable that the fly ash used is very low in calcium, which enables the development and analysis of calcium-free gel structures in the fly ash-based binder systems. The GBFS has a density of 2800 kg/m^3 and a d_{50} of 15 μm, while the fly ash has a density of 2200 kg/m^3 and a d_{50} of 12 μm.

The alkali activator was prepared by dissolution of a solid anhydrous sodium metasilicate (49.1 wt.% SiO_2 and 50.9 wt.% Na_2O, supplied by Zeobond Pty. Ltd.) in the mix water, which was then allowed to cool to room temperature prior to preparation of the specimens. The activator doses used were 8 wt.% or 12 wt.%, by total mass of precursor (i.e., 8 g or 12 g Na_2SiO_3 per 100 g FA + GBFS), as described in Table 2. It should be noted that setting and hardening did not occur satisfactorily for samples containing $\geqslant$75% fly ash at lower concentrations of metasilicate, and therefore a higher activator dose was required to achieve satisfactory strength development in the binders containing this amount of fly ash. All samples were formulated with a water/binder ratio of 0.40, and cured in sealed polypropylene tubes at 30 °C to provide a controlled curing environment under which the material would harden sufficiently rapidly, but which is not far removed from the ambient conditions prevailing in many parts of the world, and so is relevant for practical purposes.

2.2. Analytical techniques

Microstructural and chemical analysis were performed on paste samples after 14, 28, 90 and 180 days of curing, through:

- X-ray diffraction (XRD) using a Bruker D8 Advance instrument, scanning from 5°to 65° 2θ, with a 0.02° step size and 2 s/step count time.
- Fourier transform infrared (FTIR) spectroscopy, using the KBr pellet method in a Bruker Tensor 27 spectrometer, scanning 32 times from 4000 to 400 cm^{-1} at 4 cm^{-1} resolution.
- Thermogravimetry (TG), in a PerkinElmer Diamond instrument. Samples were crushed, transferred immediately to an alumina crucible, held under isothermal conditions for 60 min at 40 °C to equilibrate, and then heated 40–1000 °C at 10 °C/min in a nitrogen environment at 200 mL/min purge rate.
- Environmental scanning electron microscopy (ESEM) with energy dispersive X-ray (EDX) analysis, at an accelerating voltage of 15 kV using an FEI Quanta ESEM instrument. Paste samples were sectioned, and polished up to 1 μm surface fineness using diamond paste. Between 35 and 40 data points were collected for the elemental analysis of each sample.

3. Results and discussion

3.1. X-ray diffraction of raw materials and alkali-activated binders

The X-ray diffractograms of the anhydrous fly ash and slag are shown in Fig. 1. The unreacted fly ash shows, as main crystalline phases, quartz (SiO_2, Powder Diffraction File (PDF) # 01-079-1910), mullite ($Al_6Si_2O_{13}$, PDF# 00-015-0776), hematite (Fe_2O_3, PDF# 00-033-0664), and maghemite (Fe_2O_3, PDF# 00-039-1346). The unreacted slag shows as main crystalline phases a small amount of calcium carbonate ($CaCO_3$) in its three polymorphs (calcite, PDF# 01-071-3699; aragonite, PDF# 01-076-0606; and vaterite, PDF# 01-075-9356), associated with the superficial weathering of the slag during storage, and gypsum ($CaSO_42H_2O$, PDF# 00-033-0311). The gypsum in the slag is likely to be associated with the milling process of the granulated slag, which is conducted in a facility used for Portland cement production. Both fly ash and slag also show a broad 'hump' feature due to the amorphous component, in the case of the fly ash between $2\theta = 15°$ and 35°, and in the unreacted slag between $2\theta = 25°$ and 35°. The

Table 1
Chemical analysis by XRF (%) of the solid binder precursors. LOI is loss on ignition at 1000 °C.

Oxide (wt.%)	SiO_2	Al_2O_3	Fe_2O_3	CaO	MgO	SO_3	Na_2O	K_2O	LOI	Others
Fly ash	62.93	24.91	5.22	<0.1	1.01	0.23	0.16	1.31	2.64	1.59
Slag	33.80	13.68	0.4	42.56	5.34	0.83	0.06	0.36	1.81	1.16

Table 2
Mix proportions of the alkali-activated slag/fly ash blends.

Sample binder ratio (wt.% slag/ wt.% fly ash)	Sodium metasilicate (activator) dose relative to binder content (wt.%)
100/0	8
75/25	8
50/50	8
25/75	12
0/100	12

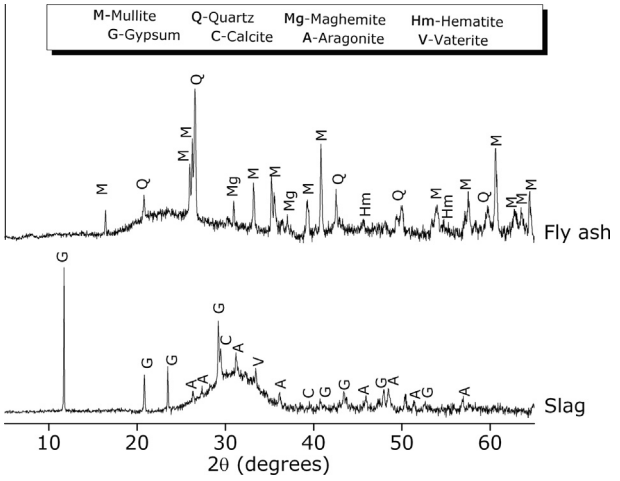

Fig. 1. X-ray diffractograms of the unreacted precursor materials used to synthesize alkali-activated slag/fly ash binders.

differences in the location of the amorphous hump are associated with the structural differences in the amorphous glasses present in the two precursors.

After alkaline activation, new crystalline reaction products are identified (Fig. 2), whose peak intensity is dependent on the slag/fly ash ratio and the time of curing. In alkali-activated slag (Fig. 2A), the main reaction product is shown near 29.5° 2θ, resembling the diffraction pattern of a poorly ordered C–S–H with a riversideite type structure (approximately $2CaSiO_3{\cdot}3H_2O$, PDF# 00-022-0600), along with traces of calcite. C–S–H type gel has previously been reported [4,12,24,26] as the main reaction product in alkali-activated slag. Calcite peaks do not show differences in intensity at the different times of curing, suggesting that this compound is a residue of the anhydrous slag. Aragonite and vaterite are also identified in the activated slag samples, consistent with the superficial carbonation of the slag used. A low intensity peak at 10° 2θ is also observed, assigned to hydrotalcite ($Mg_6Al_2(CO_3)(OH)_{16}{\cdot}4(H_2O)$, PDF# 00-041-1428)), which has also previously been identified in other alkali-activated slag systems [18,27,28].

In the sample with 75 wt.% slag/25 wt.% fly ash (Fig. 2B), disordered C-S-H type gel is also identified as a reaction product, with no significant change in the intensity of the peaks over the time of curing. The crystalline phases mullite and quartz, previously identified in the unreacted fly ash (Fig. 1), are also observed in the reacted pastes. It is not possible to identify the formation of distinct phases derived from the activation of fly ash, indicating that the structure of the gel in the 75 wt.% slag/25 wt.% fly ash blended system is mainly dominated by a C–S–H type gel and/or other disordered phases.

The structural evolution of pastes with 50 wt.% slag/50 wt.% fly ash (Fig. 2C) differs from the observations for specimens with lower contents of fly ash. In this case, an increment in the intensity of the peaks due to C–S–H type gel, along with their sharpening, is observed over the time of curing. This indicates that the kinetics of reaction of the slag upon activation are being strongly affected by the inclusion of fly ash, so that the structural evolution of the C-S-H type gel seems to be delayed at earlier age (14 days), compared with the pastes with lower contents of fly ash (Fig. 2A and B), which also promotes the formation of a C–S–H type product with a higher degree of ordering. This is consistent with the reduced Ca^{2+} availability at lower slag content, giving C–S–H phases with lower Ca/(Si + Al) ratios, and with slower formation leading to a higher degree of local structural ordering.

In pastes with 25 wt.% slag/75 wt.% fly ash (Fig. 2D), a reduced intensity of the amorphous hump (between 2θ angles 27° and 35°), associated with the formation of C–S–H type gels, is observed when compared with the samples containing a higher content of slag. Instead, a low intensity amorphous hump centered at a 2θ angle around 28° is identified, indicating the formation of a gel with a different structure. A slight increment in the intensity of this hump is observed in 28-day samples when compared with 14-day specimens. At advanced ages of curing, there is a significant reduction of the amorphous hump, along with the formation of crystalline zeolitic products with structures resembling garronite ($NaCa_{2.5}(Al_6Si_{10})O_{32}{\cdot}14H_2O$, PDF # 00-059-0383) and zeolite Na-P1 ($Na_6Al_6Si_{10}O_{32}$, PDF# 01-074-1787). These are both gismondine type structures, with differing degrees of Ca/Na substitution enabling them to be distinguished in XRD analysis.

Garronite has previously been identified in alkali-activated slag/metakaolin binders produced at high activator concentrations [29,30], and its formation seems potentially to be a consequence of the transformation of gismondine (which is the highly calcium-rich member of this family of zeolites) to garronite through an Na–Ca ion exchange process at high alkalinities. Considering that for the preparation of 25 wt.% slag/75 wt.% fly ash samples the activator concentration was increased, compared with samples including lower contents of fly ash (Table 2), it is likely that a similar process takes place here. The formation of Na-P1 (the sodium-rich endmember of the gismondine family) has previously been identified in NaOH-activated fly-ash geopolymers cured at 75 °C [31,32] and in silicate-activated fly-ash geopolymers [33]. The increased content of Na and absence of Ca in this structure are consistent with the reduced Ca availability in this binder system at the low slag content of 25 wt.%. Zeolite Na-P1 is usually formed in the early stages of hydrothermal preparation of analcime from pure silica and alumina sources at intermediate alkalinity conditions [34], and dissolves with the gradual crystallization of analcime. An increment in the alkalinity of the system then favors formation of faujasite [34] (which is often the main zeolite identified in fly ash based geopolymers [35,36]) instead of Na-P1 or analcime.

The X-ray diffractograms of the fly ash-based sample (Fig. 2E) show similar crystalline phases (quartz, mullite and hematite) to those identified in the unreacted material (Fig. 1). The formation

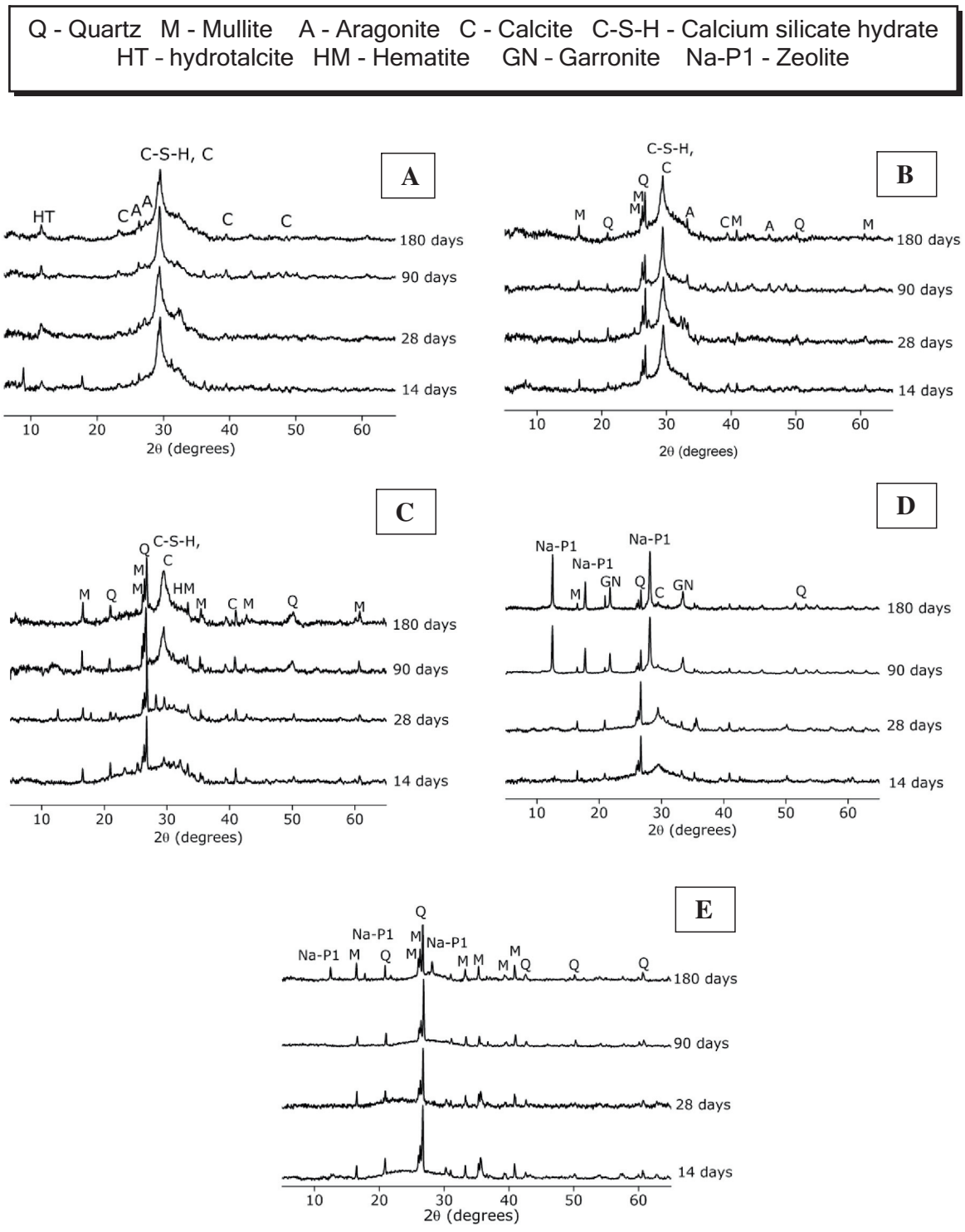

Fig. 2. X-ray diffractograms of alkali-activated slag/fly ash binders, as a function of the slag/fly ash ratio and the time of curing: (A) 100% slag, (B) 75 wt.% slag/25 wt.% fly ash, (C) 50 wt.% slag/50 wt.% fly ash, (D) 25 wt.% slag/75 wt.% fly ash and (E) 100% fly ash.

of distinctive crystalline phases is not observed between 14 and 90 days of curing; however, at 180 days, low intensity peaks consistent with Na-P1 are again observed. Considering that this particular zeolite has been observed in fly-ash based geopolymers cured for as little as 2 h at high temperatures (75 °C and 95 °C) [37], it is suggested that those regimens of curing seem to accelerate the reaction to promote the formation of a structure comparable with the structure obtained at advanced times of curing in a fly ash-based binder [38].

This analysis has provided important information regarding the ordered phases present within the alkali-activated binder systems studied. However, given that the majority of the material present is disordered, it is essential to also apply techniques which are sensitive to bonding environments in non-crystalline materials,

such as infrared spectroscopy, as discussed in the following section.

3.2. Fourier transform infrared spectroscopy (FTIR)

In show Fig. 3 shows the infrared spectra of the unreacted precursor materials used in this study, with the main bands marked. The very small vibration band observed at 1630 cm^{-1} corresponds to the bending vibration modes of H—OH bonds, while the band between 1200 and 950 cm^{-1} is associated with the asymmetric stretching vibration mode of Si—O—T bonds (T: tetrahedral Si or Al). This band is centered at 978 cm^{-1} in the slag and 1090 cm^{-1} in the fly ash, consistent with the differences in the chemical composition (Table 1) and glass structures of these materials. A reduction in the wavenumber of this band is associated with lower degrees of crosslinking of the amorphous phase of the raw materials, induced by increased contents of calcium in their structure. The shoulder at 875 cm^{-1} identified in the unreacted slag is assigned to the asymmetric stretching of AlO_4 groups present in the glass phases.

Traces of carbonates are identified in unreacted slag, associated with the asymmetric stretching mode of the O—C—O bonds of CO_3^{2-} groups [39] observed at 1480 cm^{-1}. This is consistent with the XRD results previously discussed (Fig. 1). Absorption at 670 cm^{-1} corresponds to the vibration modes of gypsum [40]. In the unreacted fly ash spectrum, the asymmetric stretching band at wavenumber 1090 cm^{-1} and the symmetric stretching band at 795 cm^{-1} are attributed to the presence of quartz. The shoulder observed at 1185 cm^{-1} and the signal between 560 and 550 cm^{-1} are associated with the octahedrally coordinated aluminum in mullite [41], as identified by XRD (Fig. 1). The band at 465 cm^{-1} is assigned to Si—O—Si bending vibration modes.

Upon activation (Fig. 4), the intensity of the broad band assigned to the stretching vibration modes of H—OH groups (between 3200 cm^{-1} and 3600 cm^{-1}) appears to increase over the time of curing, consistent with the formation of hydrated reaction products. Absorption bands at 1630–1640 cm^{-1} are assigned to the bending vibration of the O—H group of the hydrated reaction products. The spectra in Fig. 4 show particular differences in the main bands in the ranges of 600–400 cm^{-1} and 1000–900 cm^{-1} as a function of the binder formulation. In alkali-activated slag (Fig. 4A), this band is centered at 960 cm^{-1} at all times of curing assessed.

In samples with slag contents of 75% and 50% (Fig. 4B and C), the T—O—T band has shifted slightly towards lower wavenumbers compared to the unreacted slag (from 978 cm^{-1} to 970 cm^{-1} in both systems), but it is centered at higher wavenumbers than in the sample solely based on slag. This might indicate either reduced contents of Al incorporated into the C–A–S–H type gel derived from the activation of the slag in the presence of fly ash, or that

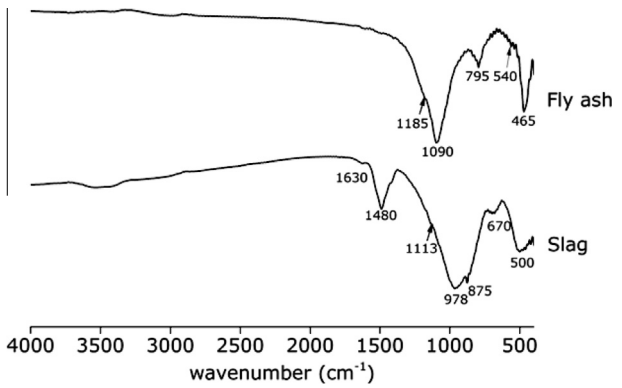

Fig. 3. FTIR spectra of the unreacted precursor materials used to synthesize alkali-activated slag/fly ash binders.

the simultaneous activation of fly ash is promoting the formation of a more crosslinked aluminosilicate type gel (also referred to as 'geopolymer gel'). Given that the fly ash is rich in Al, the latter suggestion seems far more likely. This is consistent with the observations developed through deconvolutions of ^{29}Si magic angle spinning nuclear magnetic resonance (MAS NMR) spectra for alkali-activated blends of slag and fly ash [42], where the coexistence of N–A–S–H and C–S–H type gels in blended binders was made particularly evident by the difference in the effects of carbonation on each of the gel structures. X-ray microtomography also shows similar trends in pore structure evolution for blended binders containing 50–100% slag [23], which is in good agreement with the similarity in the FTIR spectra across this compositional range as seen in Fig. 4. This is consistent with the activation conditions used, which favor the faster dissolution of Ca^{2+} in these systems, and the consequent formation of reaction products enriched in this element [43].

The inclusion of a higher fly ash content in the activated slag binders also promotes an increase in the asymmetry of the T–O–T band so that a shoulder at 1100 cm^{-1} is identified, due to the unreacted components of the fly ash (Fig. 3).

The formation of hydrotalcite, as observed by XRD (Fig. 2), is also identified by FTIR in samples solely based on slag (Fig. 4A), and those including 75 wt.% slag (Fig. 4B), with stretching vibration modes of the Al—O and Mg—O bonds at 1060 cm^{-1} and bending modes at 617 cm^{-1} [44]. This indicated that the inclusion of low percentages of fly ash (lower than 25%) is not affecting the products of the activation reaction of slag. Conversely, the distinctive hydrotalcite peak at 1060 cm^{-1} is not identified in pastes including 50 wt.% of fly ash or more, along with a shift of the Al—O and Mg—O bending modes towards higher wavenumbers (670 cm^{-1}), suggesting that the inclusion of fly ash is inducing structural changes which hinder the formation of hydrotalcite, probably related to the formation of the N–A–S–H type gel which incorporates the Al and renders it unavailable for hydrotalcite crystallization. The broad CO_3^{2-} absorption band between 1400 cm^{-1} and 1550 cm^{-1} is also observed in the activated slag/fly ash blends with contents of fly ash up to 50 wt.% (Fig. 4A–C), and is attributed to the remnant unreacted slag.

Upon activation of blended pastes containing mainly fly ash (75–100 wt.%; Fig. 4D and E), the position of the T–O–T band shifts towards higher wavenumber compared with the blended systems enriched in slag, consistent with the formation of a dominant binding gel with a lower content of Ca and a higher degree of crosslinking in this system. The shift of the T–O–T band from 1003 cm^{-1} to 1020 cm^{-1} during curing can be attributed to a progressive increase in the overall degree of crosslinking of the gel over time, potentially through the initial formation of a C–S–H type gel followed by more gradual development of an N–A–S–H type gel with a higher crosslinking degree. The final position of this band is at a slightly lower wavenumber than in the system based solely on fly ash (Fig. 4E), indicating that the presence of calcium does lead to some differences in the gel network structure. Symmetric stretching vibrations of Si—O—Si and Al—O—Si can also be identified near 740 cm^{-1}, and bending vibration of Si—O—Si and O—Si—O in the 450 cm^{-1} region. These results are consistent with the formation of a Ca^{2+}-containing N–A–S–H type gel [45].

Despite the evident inclusion of Ca^{2+} into the N–A–S–H gel in the 25 wt.% slag/75 wt.% fly ash blended system, it is apparent from Fig. 4D that an N–A–S–H type gel is the dominant reaction product in this binder. This is in agreement with observations for alkali-activated slag/metakaolin blended pastes of comparable composition [46,47]. The higher alkalinity (12% activator to binder ratio) used for the production of these binders also favors the dissolution of silicate and aluminate species from the fly ash, and it is likely that this affects the availability of calcium from the slag (which

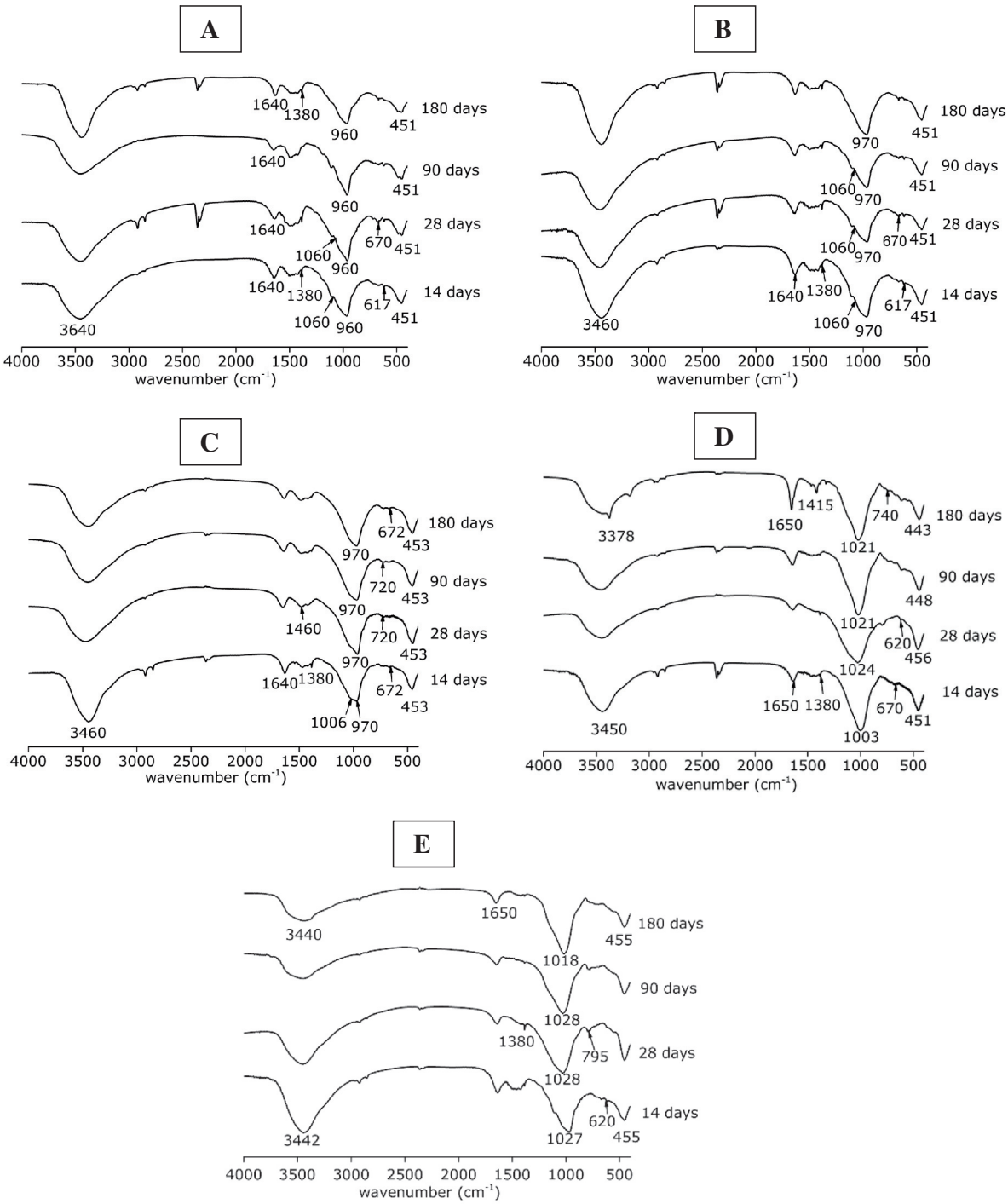

Fig. 4. FTIR spectra of alkali-activated slag/fly ash binders, as a function of the slag/fly ash ratio and the time of curing: (A) 100% slag, (B) 75 wt.% slag/25 wt.% fly ash, (C) 50 wt.% slag/50 wt.% fly ash, (D) 25 wt.% slag/75 wt.% fly ash and (E) 100% fly ash.

is suppressed at very high pH), leading to the predominance of the formation of a low-calcium N–(C)–A–S–H type gel.

Based on this understanding of the gel network structures, it is desirable to further understand the non-framework components of the gel, and particularly the water environments, which can be probed using thermal analysis as implemented in the following section.

3.3. Differential thermogravimetry

The differential thermograms (DTG) of all samples assessed, as a function of curing time and mix design, are shown in Fig. 5. Physically bound water in the gel structure (mainly in the pore network) is released at temperatures below 120 °C [48], as shown by the peak in this region. All samples show an increase in the temperature of this peak over the time of curing, suggesting the formation of gels with more tightly bonded water and/or smaller pores [49,50] as the reaction products evolve. In the activated slag sample (Fig. 5A), the first DTG peak shifts from 102 °C (14 days) to 118 °C (180 days). Similar results are observed in the 75 wt.% slag/25 wt.% fly ash and 50 wt.% slag/50 wt.% fly ash samples (Fig. 5B and C), which show further shifting of this peak towards higher temperatures at longer times of curing. The DTG results suggest that the hybrid binding phase forming in these blended

systems contains water which is bonded similarly to its environment in an alkali-activated slag binder. Detailed characterization of the response of these gels to various drying environments [51] has also shown a relatively similar water environment in the 100 wt.% and 50 wt.% slag binders.

In the higher-fly ash samples (25 wt.% slag/75 wt.% fly ash, Fig. 5D. and 100% fly ash, Fig. 5E), dehydration of the gel through loss of loosely bound water occurs at similar temperatures at early times of curing (~128 °C), shifting toward higher temperatures with longer curing. This can be attributed to the formation of Na-P1 zeolite in these specimens, as identified through XRD (Fig. 2D and E), which reports mass loss at temperatures below 200 °C as a double peak at ~90 °C and ~160 °C [52], and also a minor mass loss around 700 °C consistent with the minor peak identified in the 25 wt.% slag/75 wt.% fly ash paste (Fig. 5D) after 180 days of curing. The fact that the fly ash geopolymer specimen (Fig. 5E) shows less variation in the position of the first mass loss peak as a function of the time of curing is in good agreement with the

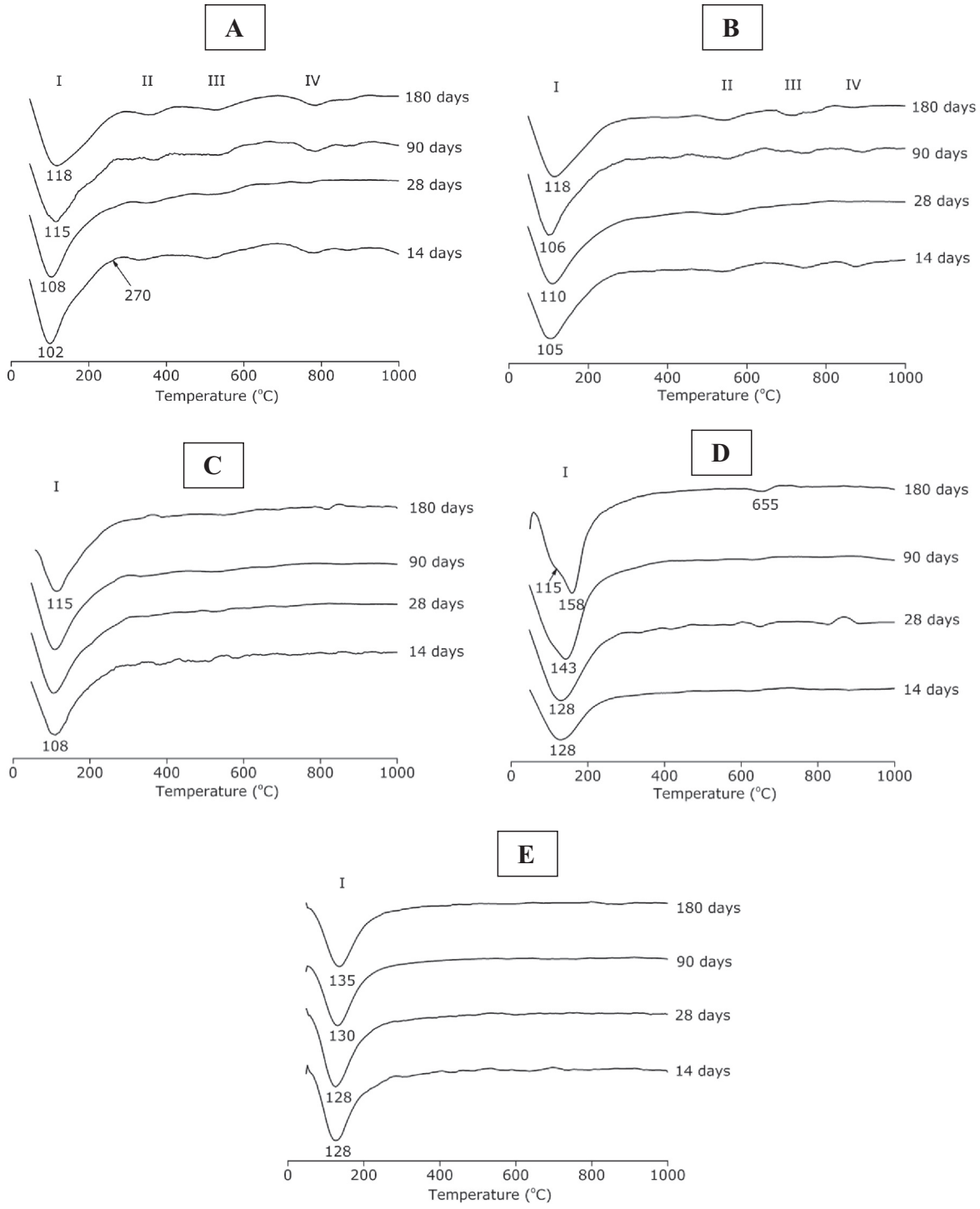

Fig. 5. Differential thermograms (DTG) of activated slag/fly ash binders, as a function of the slag/fly ash ratio and the time of curing: (A) 100% slag, (B) 75 wt.% slag/25 wt.% fly ash, (C) 50 wt.% slag/50 wt.% fly ash, (D) 25 wt.% slag/75 wt.% fly ash and (E) 100% fly ash.

formation of lower contents of Na-P1 zeolite in this specimen than with 25 wt.% slag. It should also be noted that the very loosely bound water which is held in large pores in these binders in the as-cured state tends to be released during the pre-equilibration step of the thermogravimetry experiments [51] , and so does not register in the DTG data in Fig. 5.

The peaks located at ~270 °C and at ~330 °C (region II, Fig. 5A) in the alkali-activated slag sample correspond to the dehydration of hydrotalcite [28]. The onset of calcium carbonate decomposition can also be seen between 550 °C and 600 °C (region III) in this sample, and mass loss continues at location IV (750–800 °C) corresponding to the decomposition of calcite. Similar features are observed in activated 75 wt.% slag/25 wt.% fly ash binders (Fig. 5B). With the reduction of slag content in the binder, the mass loss associated with the decomposition of carbonate phases is no longer identified. This is in good agreement with the fact that the $CaCO_3$ observed in these specimens is attributed to the weathering of the anhydrous slag during storage, and so is less prevalent at lower slag content. The thermogravimetry results confirm that portlandite is not formed in activated slag/fly ash binders, as a consequence of the high silica and alumina availability in alkali-activated binders favoring the formation of C–A–S–H type gels.

It is also desirable to understand the distribution of these gels, and the unreacted precursor particles, within the heterogeneous binder structures. To this end, the application of electron microscopy is important, as described in the following section.

3.4. SEM/EDX analysis

Backscattered electron (BSE) imaging of a 28-day cured alkali-activated slag (Fig. 6A) shows well-distributed paste areas (darker gray regions), with embedded unreacted anhydrous slag particles (light gray). It is also observed that the smaller slag grains have fully reacted at this time of curing. Compared with the fly ash-based binder (Fig. 6B), it seems that the binding paste in the alkali-activated slag is denser and presents a more homogeneous morphology, while the fly ash geopolymer shows heterogeneously distributed cavities (black) both inside and outside the remnant fly ash particles, indicating a more porous microstructure. These are commonly observed microstructural features of binders based solely on alkali-activated slag and fly ash [12,17].

The gel areas of fly ash geopolymer show notably different morphological features compared to alkali-activated slag, which is associated with the different mineralogy and shapes of the fly ash particles, and in particular the differences in solubility and reaction product gel nature between the two precursors. The porous rims surrounding the fly ash particles (circled in Fig. 6B) give evidence for ongoing reaction and gel evolution following the hardening of the binder [17]. The matrix consists of fly ash spheres of different sizes, along with pores, indicating incomplete reaction of the fly ash particles. It is also possible to observe some partially dissolved bright iron-rich particles attributed to the ferrite spinels present in the fly ash, which only participate to a limited extent in the activation reaction. However, the large bright particle at the bottom left of Fig. 6B shows a rough outer edge, consistent with the partial reaction of this particle, possibly as a more reactive aluminosilicate glass has been leached from within a phase-separated particle including both this and a ferrite phase [53].

In a 28-day cured alkali-activated 75 wt.% slag/25 wt.% fly ash binder (Fig. 7A), both unreacted slag (angular light gray particles) and unreacted fly ash (spherical light gray particles) are embedded within the binding matrix. The main binding phase (continuous gray regions) shows a similar dense morphology to that which is identified in alkali-activated slag (Fig. 6A), showing that the C-S-H type gel is effectively dominating the microstructure of this blended binder, as previously identified through XRD and FTIR. The smaller particles of slag and fly ash seem to be completely reacted after this curing duration.

With a higher fly ash content in the binder (50 wt.% slag/50 wt% fly ash, Fig. 7B), the binding phase seems to be less dense than in specimens with lower fly ash contents. This is consistent with the identification [23] that the geopolymer gel forming in activated fly ash-containing systems is less space-filling than the C–A–S–H product formed by activation of slag. The binding phase forming in this system does not seem to adhere as closely to the unreacted slag surfaces as is observed in pastes with lower contents of fly ash, which may mean that the reaction of the slag particles has continued for a longer duration after the hardening of the binder than was the case in the systems with a higher slag content.

Increased porosity is evident in the sample with 25 wt.% slag/75 wt.% fly ash (Fig. 7C) compared with specimens with higher contents of slag, consistent with a microstructure mostly governed by a geopolymer type gel, as previously identified through other analytical techniques discussed in this paper, as well as by X-ray microtomography [23].

EDX results obtained for multiple points selected from within the binder regions (i.e. excluding unreacted precursor particles) of the different activated slag/fly ash blended pastes studied are shown in Fig. 8. Calcium, aluminum and silicon contents of specimens with 28, 90 and 180 days of curing are reported, renormalized to 100% on an oxide basis for plotting on the ternary diagrams (i.e., neglecting the other elements present). These plots clearly show the variation in gel composition across the different slag/fly ash blended binders as a function of the time of curing, and confirm also the approximate chemical compositions of the types of gel forming with different binder proportions: the black

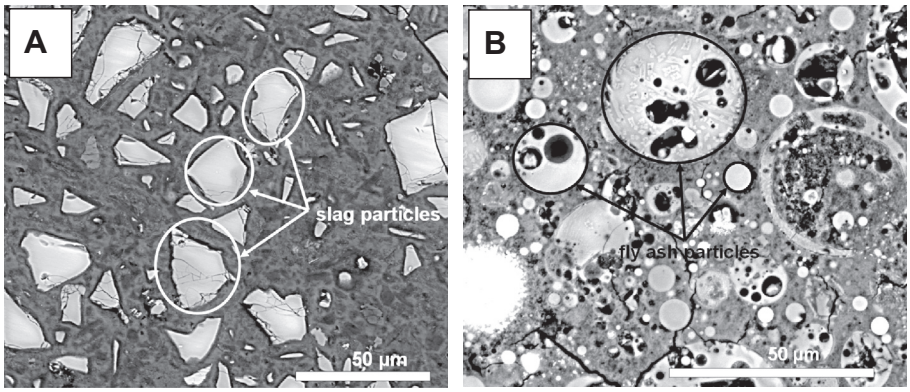

Fig. 6. BSE images of (A) alkali-activated slag, and (B) alkali-activated fly ash, after 28 days of curing.

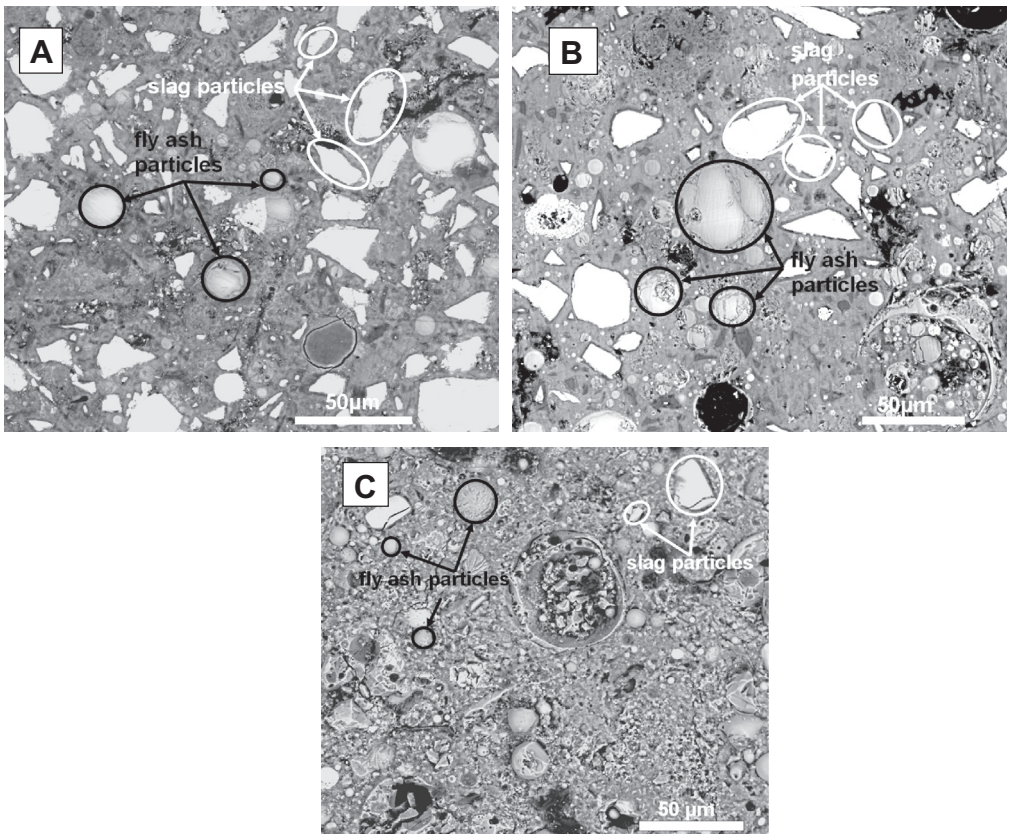

Fig. 7. BSE images of alkali-activated blended binders after 28 days of curing: (A) 75 wt.% slag/25 wt.% fly ash, (B) 50 wt.% slag/50 wt.% fly ash and (C) 25 wt.% slag/75 wt.% fly ash.

circles in Fig. 8A,B correspond to a C–A–S–H type gel, the dashed black circles in Fig. 8B–E to an N–A–S–H type gel, and the shaded circles in Fig. 8C and D are an N–(C)–A–S–H type gel.

Fig. 8A shows a clustered region of points corresponding to the C–A–S–H type gel forming in the alkali-activated slag binder, with a Ca/Si ratio between 1.02 and 1.08 and Al/Si ratios of 0.35–0.40, at 28 and 180 days respectively, consistent with what has previously been reported for similar systems [10,54]. The Al/Si atomic ratios do not exhibit significant changes at different slag/fly ash ratios and times of curing. The incorporation of fly ash in the 75 wt.% slag/25 wt.% fly ash sample (Fig. 8B) promotes the formation of two distinct gels associated with the activation reaction of both precursors. The C–A–S–H product seems to show a reduction in the content of calcium with increasing time of curing, and consequently the binder becomes enriched in aluminum and silicon, consistent with the formation of a C–N–A–S–H type product. The minor secondary binder products identified in these specimens (as seen by XRD, Fig. 2B) present a lower content of calcium than the C–N–A–S–H product mainly forming the binding gel, consistent with the slight shifting of the chemistry of the binding phases in activated slag binders due to the inclusion of fly ash. Thus, even with the inclusion of a moderate content of fly ash, the coexistence of C–A–S–H gel with a more aluminosilicate-type gel is feasible, as suggested by other studies [11,21,42]. However, it seems that these gels do not remain independent of each other on the length scale probed by ESEM/EDX, but instead they are intermixing towards the formation of a third, hybrid binding phase. This is consistent with the trends which have been identified in synthetic C–A–S–H and N–A–S–H type gels [55].

The inclusion of 50 wt.% fly ash (Fig. 8C) leads to the formation of a binder gel with a composition intermediate between a C–A–S–H product identified in slag-based binders, and an N–A–S–H type geopolymer gel. This binding product may be formed through the incorporation of calcium in the N–A–S–H gel derived from the activation of fly ash, and/or the incorporation of sodium in the C–A–S–H product formed from the activation of the slag – or it may be that these two types of gel are still chemically distinct but become intermixed on a length scale too short to measure by ESEM/EDX. Under the alkalinity conditions used for the production of these specimens, it has been observed throughout this study, and elsewhere [23], that the binders with up to 50 wt.% fly ash show microstructural characteristics resembling alkali-activated slag binders, although the EDX results suggest that the binding phase forming in blended slag/fly ash binders presents a different chemical composition. Thus, if a hybrid C–N–A–S–H type phase is forming, it has comparable structural characteristics to C–A–S–H products.

In the sample with 25 wt.% slag/75 wt.% fly ash (Fig. 8D) and the fly ash-based binder (Fig. 8E), a distinct C–(N)–A–S–H product is no longer identified. Instead, the binding phases observed are a gel with a low content of calcium that can be described as an N–(C)–A–S–H product in the 25% slag system, along with geopolymer-type gel (N–A–S–H) in the 25% slag and pure fly ash systems. The low Ca/Si ratios exhibited by these gels are consistent with the FTIR spectra, which suggested the reduction of calcium concentration within the binding phase, along with formation of a product with higher degrees of crosslinking. These results confirm that in activated blended systems with high contents of fly ash, the microstructure is mainly dominated by an N–A–S–H geopolymer type product.

4. Conclusions

The nature of the gel in alkali-activated slag/fly ash blended binders is strongly dependent on the slag/fly ash ratio, as the differences in chemistry and mineralogy of these precursors promote the formation of different binder products. A calcium silicate

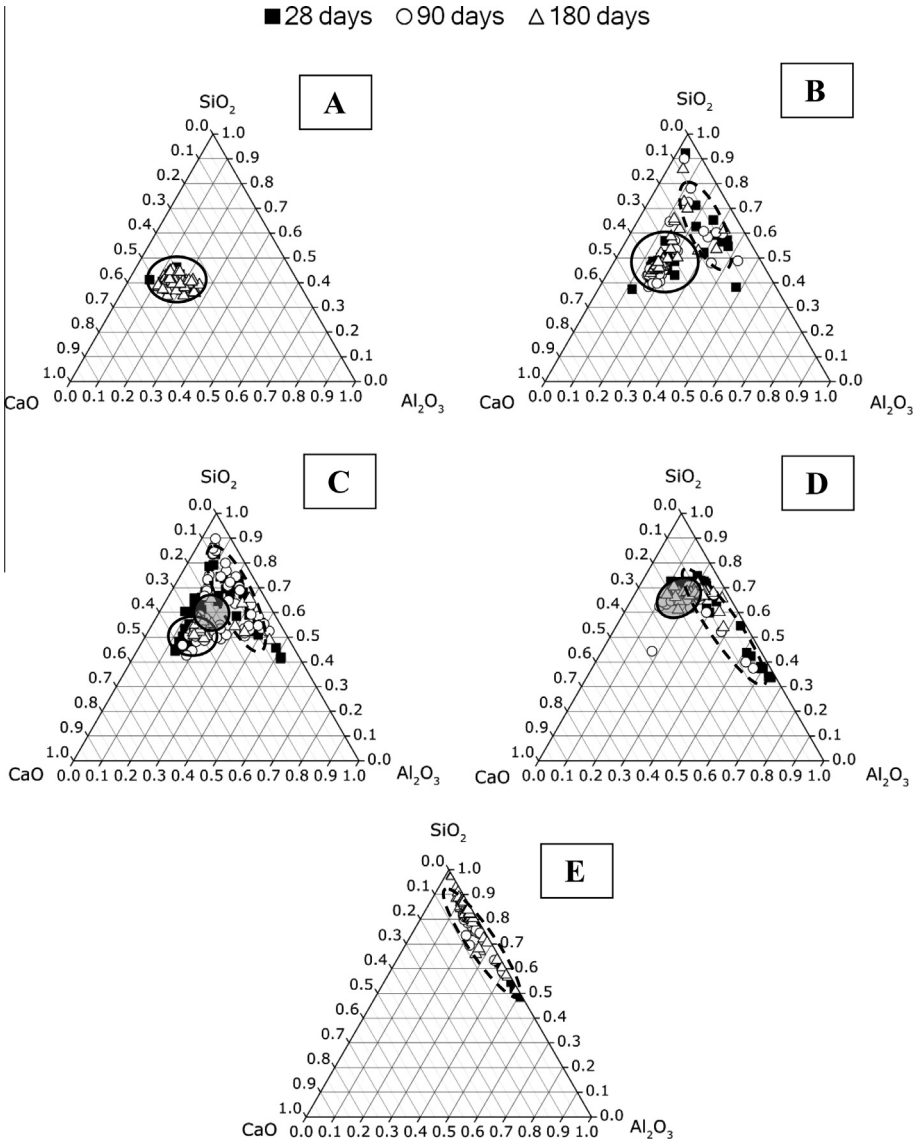

Fig. 8. Ternary representations of EDX data for alkali-activated slag/fly ash binders, as a function of the slag/fly ash ratio and the time of curing: (A) 100% slag, (B) 75 wt.% slag/25 wt.% fly ash, (C) 50 wt.% slag/50 wt.% fly ash, (D) 25 wt.% slag/75 wt.% fly ash, (E) 100% fly ash. Compositions included in the black circles correspond to a C–A–S–H type gel, dashed black circles to an N–A–S–H type gel, and black circles filled with dark gray corresponds to an N–(C)–A–S–H type gel.

hydrate gel substituted with Al and Na (C–N–A–S–H) is identified as the main binding product in geopolymer binders with contents of slag $\geqslant$50 wt.% of the total binder. With increased contents of fly ash, the systems seem to be mainly composed of a hybrid binding phase with a composition that could be described as an N–C–A–S–H type gel, with water more tightly bound (i.e. held in smaller pores) and a higher degree of crosslinking than identified in C–A–S–H type gel forming in activated slag binders.

This study provides strong evidence of different mechanisms of calcium release from slag upon activation in the presence of aluminosilicate precursor. Partial substitution of slag in fly ash geopolymer slows down the formation of C–A–S–H binding gel as the consequence of Al and Si release over time along with the formation of hybrid C–N–A–S–H gels. This study also shows that an increase in the content of fly ash as a low-calcium aluminosilicate source promotes the formation of zeolites in a hybrid gel system beyond 28 days, which usually occurs at higher curing temperatures in the presence of a lower activator concentration. This characterization of samples after longer ages of curing has enhanced our insight in the mechanism of formation of binding gels and other phases. Such micro-scale understanding is essential for predicting the macro-scale mechanical strength and durability performance of alkali-activated materials.

Acknowledgments

The authors acknowledge the Malaysian Ministry of Higher Education for funding of this project through the Melbourne-Malaysia Split Ph.D. program. This study has also been supported by the Australian Research Council, through a Linkage Project grant co-sponsored by Zeobond Research, and via the Discovery Grants program, including some support through the Particulate Fluids Processing Centre. Support provided by the Faculty of Engineering, University of Sheffield, is also gratefully acknowledged.

References

[1] Juenger MCG, Winnefeld F, Provis JL, Ideker JH. Advances in alternative cementitious binders. Cem Concr Res 2011;41(12):1232–43.

[2] van Deventer JSJ, Provis JL, Duxson P. Technical and commercial progress in the adoption of geopolymer cement. Min Eng 2012;29:89–104.
[3] van Deventer JSJ, Provis JL, Duxson P, Brice DG. Chemical research and climate change as drivers in the commercial adoption of alkali activated materials. Waste Biomass Valor 2010;1:145–55.
[4] Bakharev T, Sanjayan JG, Cheng Y-B. Alkali activation of Australian slag cements. Cem Concr Res 1999;29(1):113–20.
[5] van Jaarsveld JGS, van Deventer JSJ. Effect of the alkali metal activator on the properties of fly ash-based geopolymers. Ind Eng Chem Res 1999;38:3932–41.
[6] Roy DM. Alkali-activated cements: opportunities and challenges. Cem Concr Res 1999;29(2):249–54.
[7] Palomo A, Grutzeck MW, Blanco MT. Alkali-activated fly ashes: A cement for the future. Cem Concr Res 1999;29(8):1323–9.
[8] Gruskovnjak A, Lothenbach B, Holzer L, Figi R, Winnefeld F. Hydration of alkali-activated slag: comparison with ordinary Portland cement. Adv Cem Res 2006;18(3):119–28.
[9] Sindhunata, Provis JL, Lukey GC, Xu H, Van Deventer JSJ. Structural evolution of fly ash based geopolymers in alkaline environments. Ind Eng Chem Res 2008;47(9):2991–9.
[10] Richardson IG, Brough AR, Groves GW, Dobson CM. The characterization of hardened alkali-activated blast-furnace slag pastes and the nature of the calcium silicate hydrate (C-S-H) phase. Cem Concr Res 1994;24(5):813–29.
[11] Puertas F, Palacios M, Manzano H, Dolado JS, Rico A, Rodríguez J. A model for the C–A–S–H gel formed in alkali-activated slag cements. J Eur Ceram Soc 2011;31(12):2043–56.
[12] Brough AR, Atkinson A. Sodium silicate-based, alkali-activated slag mortars: Part I. Strength, hydration and microstructure. Cem Concr Res 2002;32(6):865–79.
[13] Roy DM, Jiang W, Silsbee MR. Chloride diffusion in ordinary, blended, and alkali-activated cement pastes and its relation to other properties. Cem Concr Res 2000;30(12):1879–84.
[14] Bakharev T, Sanjayan JG, Cheng YB. Sulfate attack on alkali-activated slag concrete. Cem Concr Res 2002;32(2):211–6.
[15] Ravikumar D, Peethamparan S, Neithalath N. Structure and strength of NaOH activated concretes containing fly ash or GGBFS as the sole binder. Cem Concr Compos 2010;32(6):399–410.
[16] Bernal SA, Mejía de Gutiérrez R, Provis JL. Engineering and durability properties of concretes based on alkali-activated granulated blast furnace slag/metakaolin blends. Constr Build Mater 2012;33:99–108.
[17] Fernández-Jiménez A, Palomo A, Criado M. Microstructure development of alkali-activated fly ash cement: a descriptive model. Cem Concr Res 2005;35(6):1204–9.
[18] Oh JE, Monteiro PJM, Jun SS, Choi S, Clark SM. The evolution of strength and crystalline phases for alkali-activated ground blast furnace slag and fly ash-based geopolymers. Cem Concr Res 2011;40(2):189–96.
[19] Lloyd R.R. The durability of inorganic polymer cements, PhD thesis. University of Melbourne; 2008.
[20] Escalante García JI, Campos-Venegas K, Gorokhovsky A, Fernández A. Cementitious composites of pulverised fuel ash and blast furnace slag activated by sodium silicate: effect of Na2O concentration and modulus. Adv Appl Ceram 2006;105(4):201–8.
[21] Kumar S, Kumar R, Mehrotra SP. Influence of granulated blast furnace slag on the reaction, structure and properties of fly ash based geopolymer. J Mater Sci 2010;45(3):607–15.
[22] Puligilla S, Mondal P. Role of slag in microstructural development and hardening of fly ash-slag geopolymer. Cem Concr Res 2013;43:70–80.
[23] Provis JL, Myers RJ, White CE, Rose V, van Deventer JSJ. X-ray microtomography shows pore structure and tortuosity in alkali-activated binders. Cem Concr Res 2012;42(6):855–64.
[24] Yang T, Yao X, Zhang Z, Wang H. Mechanical property and structure of alkali-activated fly ash and slag blends. J Sust Cem-Based Mater 2012;1(4):167–78.
[25] Xu H, Provis JL, van Deventer JSJ, Krivenko PV. Characterization of aged slag concretes. ACI Mater J 2008;105(2):131–9.
[26] Wang SD, Scrivener KL. Hydration products of alkali activated slag cement. Cem Concr Res 1995;25(3):561–71.
[27] Puertas F, Fernández-Jiménez A. Mineralogical and microstructural characterisation of alkali-activated fly ash/slag pastes. Cem Concr Compos 2003;25(3):287–92.
[28] Ben Haha M, Lothenbach B, Le Saout G, Winnefeld F. Influence of slag chemistry on the hydration of alkali-activated blast-furnace slag - Part I: Effect of MgO. Cem Concr Res 2011;41(9):955–63.
[29] Zhang YJ, Wang YC, Xu DL, Li S. Mechanical performance and hydration mechanism of geopolymer composite reinforced by resin. Mater Sci Eng A 2010;527(24–25):6574–80.
[30] Bernal SA, Provis JL, Rose V, Mejía de Gutiérrez R. High-resolution X-ray diffraction and fluorescence microscopy characterization of alkali-activated slag-metakaolin binders. J Am Ceram Soc 2013;96(6):1951–7.
[31] Guo X, Shi H, Dick WA. Compressive strength and microstructural characteristics of class C fly ash geopolymer. Cem Concr Compos 2010;32(2):142–7.
[32] Bakharev T. Geopolymeric materials prepared using Class F fly ash and elevated temperature curing. Cem Concr Res 2005;35(6):1224–32.
[33] Rodríguez ED, Bernal SA, Provis JL, Paya J, Monzo JM, Borrachero MV. Effect of nanosilica-based activators on the performance of an alkali-activated fly ash binder. Cem Concr Compos 2013;35(1):1–11.
[34] Kohoutková M, Kloužkova A, Maixner J, Mrázová M. Preparation and characterization of analcime powders by X-ray and SEM analyses. Ceram-Silik 2007;51(1):9–14.
[35] Fernández-Jiménez A, Monzó M, Vicent M, Barba A, Palomo A. Alkaline activation of metakaolin–fly ash mixtures: obtain of zeoceramics and zeocements. Micropor Mesopor Mater 2008;108(1–3):41–9.
[36] Criado M, Fernández-Jiménez A, de la Torre AG, Aranda MAG, Palomo A. An XRD study of the effect of the SiO_2/Na_2O ratio on the alkali activation of fly ash. Cem Concr Res 2007;37(5):671–9.
[37] Bakharev T. Thermal behaviour of geopolymers prepared using class F fly ash and elevated temperature curing. Cem Concr Res 2006;36(6):1134–47.
[38] Lloyd RR. Accelerated ageing of geopolymers. In: Provis JL, van Deventer JSJ, editors. Geopolymers: structure, processing, properties and industrial applications. Cambridge, UK: Woodhead; 2009. p. 139–66.
[39] Reig FB, Adelantado JVG, Moya Moreno MCM. FTIR quantitative analysis of calcium carbonate (calcite) and silica (quartz) mixtures using the constant ratio method. Application to geological samples. Talanta 2002;58(4):811–21.
[40] Gadsden JA. Infrared spectra of minerals and related inorganic compounds. London: Butterworths; 1975.
[41] Beran A, Voll D, Schneider H. Dehydration and structural development of mullite precursors: an FTIR spectroscopic study. J Eur Ceram Soc 2001;21(14):2479–85.
[42] Bernal SA, Provis JL, Walkley B, San Nicolas R, Gehman JD, Brice DG. Gel nanostructure in alkali-activated binders based on slag and fly ash and effects of accelerated carbonation. Cem Concr Res 2013.
[43] García Lodeiro I, Fernández-Jimenez A, Palomo A, Macphee DE. Effect on fresh C–S–H gels of the simultaneous addition of alkali and aluminium. Cem Concr Res. 2010;40(1):27–32.
[44] López T, Bosch P, Asomoza M, Gómez R, Ramos E. DTA-TGA and FTIR spectroscopies of sol-gel hydrotalcites: aluminum source effect on physicochemical properties. Mater Lett 1997;31(3–6):311–6.
[45] Criado M, Fernández-Jiménez A, Palomo A. Alkali activation of fly ash: Effect of the SiO2/Na2O ratio. Part I: FTIR study. Micropor Mesopor Mater 2007;106(1-3):180–91.
[46] Bernal SA, Rodríguez ED, Mejía de Gutierrez R, Gordillo M, Provis JL. Mechanical and thermal characterisation of geopolymers based on silicate-activated metakaolin/slag blends. J Mater Sci 2011;46(16):5477–86.
[47] Bernal SA, Rodríguez ED, Mejia de Gutiérrez R, Provis JL, Delvasto S. Activation of metakaolin/slag blends using alkaline solutions based on chemically modified silica fume and rice husk ash. Waste Biomass Valor 2012;3(1):99–108.
[48] Alarcon-Ruiz L, Platret G, Massieu E, Ehrlacher A. The use of thermal analysis in assessing the effect of temperature on a cement paste. Cem Concr Res 2005;35(3):609–13.
[49] Abdelrazig BEI, Main SD, Nowell DV. Hydration studies of modified OPC pastes by differential scanning calorimetry and thermogravimetry. J Therm Anal 1992;38(3):495–504.
[50] Nochaiya T, Wongkeo W, Pimraksa K, Chaipanich A. Microstructural, physical, and thermal analyses of Portland cement–fly ash–calcium hydroxide blended pastes. J Therm Anal Calorim 2010;100(1):101–8.
[51] Ismail I, Bernal SA, Provis JL, Hamdan S, van Deventer JSJ. Drying-induced changes in the structure of activated pastes. J Mater Sci. 2013;48:3566–77.
[52] Majchrzak-Kucęba I, Nowak W. Thermal analysis of fly ash-based zeolites. J Therm Anal Calorim 2004;77(1):125–31.
[53] Lloyd RR, Provis JL, van Deventer JSJ. Microscopy and microanalysis of inorganic polymer cements. 1: Remnant fly ash particles. J Mater Sci 2009;44(2):608–19.
[54] Escalante-Garcia JI, Fuentes AF, Gorokhovsky A, Fraire-Luna PE, Mendoza-Suarez G. Hydration products and reactivity of blast-furnace slag activated by various alkalis. J Am Ceram Soc 2003;86(12):2148–53.
[55] García-Lodeiro I, Palomo A, Fernández-Jiménez A, Macphee DE. Compatibility studies between N–A–S–H and C–A–S–H gels. Study in the ternary diagram $Na_2O–CaO–Al_2O_3–SiO_2–H_2O$. Cem Concr Res 2011;41(9):923–31.